Hydrol. Earth Syst. Sci. Discuss., 12, 5123–5149, 2015
www.hydrol-earth-syst-sci-discuss.net/12/5123/2015/
doi:10.5194/hessd-12-5123-2015

Hydrology and Earth System Sciences
Open Access
Discussions

Optimality and inference in hydrology from entropy production considerations: synthetic hillslope numerical experiments

S. J. Kollet[1,2]

[1]IBG-3, Institute for Bio- and Geosciences, Research Centre Jülich, Jülich, Germany
[2]Centre for High-Performance Scientific Computing in Terrestrial Systems, Geoverbund ABC/J, Jülich, Germany

Received: 26 April 2015 – Accepted: 2 May 2015 – Published: 29 May 2015

Correspondence to: S. J. Kollet (s.kollet@fz-juelich.de)

Published by Copernicus Publications on behalf of the European Geosciences Union.

Abstract

In this study, entropy production optimization and inference principles are applied to a synthetic semi-arid hillslope in high-resolution, physics-based simulations. The results suggest that entropy or power is indeed maximized, because of the strong nonlinearity of variably saturated flow and competing processes related to soil moisture fluxes, the depletion of gradients, and the movement of a free water table. Thus, it appears that the maximum entropy production (MEP) principle may indeed be applicable to hydrologic systems. In the application to hydrologic system, the free water table constitutes an important degree of freedom in the optimization of entropy production and may also relate the theory to actual observations. In an ensuing analysis, an attempt is made to transfer the complex, "microscopic" hillslope model into a macroscopic model of reduced complexity using the MEP principle as an interference tool to obtain effective conductance coefficients and forces/gradients. The results demonstrate a new approach for the application of MEP to hydrologic systems and may form the basis for fruitful discussions and research in future.

1 Introduction

Theories of optimality and self-organization are appealing when dealing with complex non-linear systems, because of their usefulness in interpreting interactions of gradients and fluxes; inferring effective exchange coefficients, conductances, and up-/downscaling; and ultimately in quantifying (predicting) systems' states and uncertainties. In this context, entropy production and entropy production optimization (mini-/maximization) received attention, because of the principles' physics-based foundation in non-equilibrium thermodynamics and potential connection with information theory (e.g., Dewar, 2003; Koutsoyiannis, 2014). These principles appear to be useful in applications to hydrologic (e.g., Zehe et al., 2013; Ehret et al., 2014), ecohydrologic (e.g., Dewar, 2010; Miedziejko and Kedziora, 2014; del Jesus et al.,

HESSD
12, 5123–5149, 2015

2012), and atmospheric sciences (e.g., Paillard and Herbert, 2013), and in general to open complex nonlinear thermodynamical systems (Abe and Okuyama, 2011).

The principle of entropy production optimization (EPO) states that in an open system, a dynamic equilibrium is obtained, when entropy production inside (due to e.g. flow processes of heat and water) equals the net entropy exchange with the outside. Optimality of the dynamic equilibrium is obtained, because the gradient, which drives the flux and, thus the production of entropy, is reciprocally depleted by the same flux (Kleidon et al., 2013). Note also, dynamic equilibrium refers to a state of stationarity in the statistical sense. In this study, this is essential, in order to discuss nonlinear systems, which are forced by a periodic boundary condition and are not well-mixed.

In hydrology, the EPO principle has been applied to conceptual problems based on the overarching rational that entropy production is maximized (maximum entropy production, MEP) in obtaining a state of dynamic equilibrium by optimizing the fluxes and gradients in competition via an adjustment of the conductance, λ. Following Kleidon (2010)

$$\sigma = \rho Q \frac{\mu_{\text{high}} - \mu_{\text{low}}}{T}, \tag{1}$$

where σ is the entropy production ($\mathrm{M T^{-2} K^{-1}}$); μ_{high} and μ_{low} are a high and low chemical potentials, respectively ($\mathrm{L^2 T^{-2}}$); ρ is the density of water ($\mathrm{M L^{-3}}$); T is temperature (K); and Q is the volume flow rate ($\mathrm{L^3 T^{-1}}$). Because in this study, only isothermal conditions are considered, power P, is used interchangeably with entropy production (Westhoff and Zehe, 2013; Westhoff et al., 2014) and chemical potential is replaced with the hydraulic head normalized by the specific weight of water leading to

$$P = q\,(H_{\text{h}} - H_{\text{l}}), \tag{2}$$

$$q = \lambda\,(H_{\text{h}} - H_{\text{l}}), \tag{3}$$

where P is power per unit area ($\mathrm{L^2 T^{-1}}$); q is the flux ($\mathrm{L T^{-1}}$); H_{h} and H_{l} are the high and low hydraulic heads, respectively (L); and λ is a hydraulic conductance coefficient

HESSD
12, 5123–5149, 2015

(T^{-1}). Note, σ and P are positive quantities per definition, and may be used in a power budget analysis to quantify net export/import of power by a flux (Schymanski et al., 2010).

There have been some studies demonstrating, how P can be optimized as a function of λ to obtain a system's state at which entropy production is indeed at its maximum. In hydrology, there are quite a few examples of the application and discussion of the MEP principle (e.g., Westhoff et al., 2014; Kleidon and Schymanski, 2008; Ehret et al., 2014) also in connection with data (e.g., Zehe et al., 2013). However, its validity and applicability to hydrologic systems is still in question (Westhoff and Zehe, 2013).

Often the MEP principle has been tested at steady state with simple linear bucket models, which are well-mixed. For example, Porada et al. (2011) performed a detailed entropy production analysis of the land surface hydrologic cycle including the shallow vadose zone assuming vertical equilibrium of the soil bucket model. Applying linear bucket models, Kleidon and Schymanski (2008) showed that if the natural system possesses enough degrees of freedom, in case of steady state, the system will tend towards a λ, when entropy production is maximized. For similar bucket models, Westhoff et al. (2014) demonstrated the impact of periodic boundary forcing on P, which may result in more than one maximum for unique λ values at dynamic equilibrium. It is exactly this principle of optimization, which could make the MEP the inference tool of choice in case of hydrologic systems. Unfortunately, the systems under consideration so far are quite conceptual and do not share the complexity and degrees of freedom of the natural terrestrial system. Thus, relating the findings from the idealized box models to the terrestrial system is difficult, because natural systems are almost never well-mixed and linear.

In the case of the critical zone, which is here defined as the shallow subsurface connecting the atmosphere with the groundwater system, significant vertical gradients may exist under dynamic equilibrium conditions; and fluxes in and out of the system are determined by nonlinear exchange coefficients and gradients, which are generated by e.g., evaporation and infiltration from the land surface (Kollet and Maxwell, 2008).

HESSD
12, 5123–5149, 2015

Thus, in order to test the MEP principle, periodic forcing of the atmosphere, resulting evaporation and infiltration from the land surface coupled with subsurface moisture transport, and groundwater flow need to be considered. This is only possible utilizing physics-based models of the terrestrial system, which have received considerable attention since the blueprint of Freeze and Harlan (1964).

For the critical zone, this study tests the MEP principle including the hypothesis that if a single atmospheric time series is repeatedly applied over a hillslope until dynamic equilibrium is reached, then the hillslope will tend toward an optimized state of exchange, when entropy or power production is maximized. In testing the hypothesis, one will also obtain insight into the dynamics and mechanisms of the critical zone to optimize entropy production. In addition, the MEP principle is applied as an inference tool to obtain effective conductance coefficients and gradients in an attempt to transfer the complex hillslope model into a conceptual model of reduced complexity.

2 Methods

In this study, the response of the critical zone along a shallow cross-section of a synthetic hillslope was simulated in 2-D using the integrated variably saturated groundwater-surface water flow model ParFlow, PF, coupled to the Common Land Model, CLM. The coupled model PF.CLM simulates variably saturated moisture transport in the subsurface coupled with land surface processes that are evaporation, net radiation, sensible heat and ground heat flux. Note, transpiration by plants was not taken into account in this study. The interested reader is referred to Kollet and Maxwell (2008) for detailed explanation of the model. At the top, PF.CLM is forced with an hourly atmospheric time series of one year consisting of long and short wave radiation, air temperature, precipitation, wind speed, specific humidity, and barometric pressure over one year in spinup mode. The time series was derived from Kollet and Maxwell (2008) by reducing the rainfall rates consistently by about 30 % to obtain semi-arid conditions. The time series' mean annual temperature and precipitation are 291 K and

HESSD
12, 5123–5149, 2015

637 mm, respectively. The PF.CLM source code and input data used in the numerical experiments outlined below can be obtained from the author.

2.1 Model setup and numerical experiments

The synthetic hillslope was simulated to a depth of some 5 m along a 100 m cross-section with a constant lateral and vertical resolution of 1 m and 1 cm, respectively. A constant topographic slope of 0.001 % was implemented in the finite difference framework with respect to a horizontal bottom of the cross-section. The van Genuchten relationship was used for the relative hydraulic conductivity $k_r(p)$ [–] and saturation $\theta(p)$ [–] functions, where p [L] is the hydraulic pressure of the porous medium. The constant hydraulic parameters of the numerical experiment are van Genuchten's $n = 2$ and alpha = 2 [m^{-1}]; porosity, $\varphi = 0.44$ [–]. The boundary conditions were no-flow at the bottom, and at $x = 0$ and $x = 100$ m, and of the free-surface overland flow type (Kollet and Maxwell, 2006) at the top. All experiments were initialized with an arbitrary pressure distribution and run repeatedly with the aforementioned atmospheric yearly time series with a time step of 1 h until dynamic equilibrium was reached (statistical steady state).

In order identify an optimum in P as a function of an effective conductance coefficient, which is not known at this point, saturated hydraulic conductivity, K_{sat}, was very varied under the assumption that K_{sat} is proportional to the effective conductance coefficient. (This assumption is tested in Sect. 3.2.) Two series of numerical experiments, S1 and S2, were performed. In S1, the saturated hydraulic conductivity was varied K_{sat} = [0.0005, 0.001, 0.005, 0.01, 0.05, 0.5, 0.1, 1.0, 10.0] [$m\,h^{-1}$]. In S2, K_{sat} was varied exactly the same way as in S1, but the values were perturbed spatially with white noise using a log-normal distribution with one order of magnitude standard deviation (SD). Note, the perturbations for the different K_{sat} values were performed with the same seed in order to generate identically spatial random patterns.

HESSD
12, 5123–5149, 2015

2.2 Analyses

In addition to standard fluxes and states, such as the total water budget, evaporation, q^{ev} (LT^{-1}), infiltration, q^{inf} (LT^{-1}), hydraulic head, H (L), the variables defined below were calculated in order to arrive at a detailed power analysis for the subsurface. While overland flow occurred in the numerical experiment by the process of excess infiltration and also shallow excess saturation, surface runoff out of the domain and resulting power was not included in the analysis. Runoff out of the domain occurred only for $K_{sat} = 0.0005\ (m\,h^{-1})$ and S2 and was only 2.2 % of the annual precipitation. For consistency, the contribution to infiltration by surface runoff (or runon) from neighboring cells at the land surface was incorporated in the water and power budget analyses.

At the land surface, net exfiltration/infiltration, $\overline{q}^{ex,inf}$ ($m\,a^{-1}$), over the simulation period are calculated as the sum of the hourly differences between precipitation, PCP ($m\,h^{-1}$), and evaporation, E ($m\,h^{-1}$), at each grid point along the x direction with indices i

$$\overline{q}_i^{ev,inf} = -\sum_{n=1}^{NT} PCP_i^n - E_i^n, \tag{4}$$

where NT is the total number of time steps. These net fluxes can be integrated over regions of the domain to identify net recharge and discharge areas along the land surface

$$\overline{q}^{ev,inf} = \sum_{i}^{NI} \overline{q}_i^{ev,inf}, \tag{5}$$

where NI is the upper bound of a region in the x direction.

HESSD
12, 5123–5149, 2015

Annual mean hydraulic head values at each pixel, $\overline{H}_{i,k}$ (m), are obtained in a similar fashion

$$\overline{H}_{i,k} = \frac{1}{\mathrm{NT}} \sum_{n=1}^{\mathrm{NT}} H_{i,k}^{n}. \tag{6}$$

Power across each cell interface generated by the fluxes in the east, west, up, and down direction is indicated with the subscripts e, w, u, and d, respectively, and is calculated based on the equation

$$\begin{aligned} P_{\mathrm{e}} &= \lambda_{\mathrm{e}} \left(H_{\mathrm{e}} - H_{i,j}\right)^2 \\ P_{\mathrm{w}} &= \lambda_{\mathrm{w}} \left(H_{\mathrm{w}} - H_{i,j}\right)^2 \\ P_{\mathrm{u}} &= \lambda_{\mathrm{u}} \left(H_{\mathrm{u}} - H_{i,j}\right)^2 \\ P_{\mathrm{d}} &= \lambda_{\mathrm{d}} \left(H_{\mathrm{d}} - H_{i,j}\right)^2 \end{aligned} \tag{7}$$

The interface conductances, λ, are calculated following

$$\lambda_{\mathrm{e,\,w}} = \frac{K_{\mathrm{sat,\,harm}} k_{\mathrm{r,\,uw}}}{\Delta x};\ \lambda_{n,s} = \frac{K_{\mathrm{sat,\,harm}} k_{\mathrm{r,\,uw}}}{\Delta z} \tag{8}$$

with $K_{\mathrm{sat,\,harm}}$ being the harmonic average of the two adjacent cell hydraulic conductivities; $k_{\mathrm{r,\,uw}}$ is the upwinded relative hydraulic conductivity; and Δx and Δz are the spatial discretizations in the x and z direction, respectively, which are constant in this study. Thus, the calculation of power is consistent with the way PF.CLM calculates the Darcy fluxes based on a finite control volume discretization with two-point flux approximation.

Using Eq. (4), the instantaneous power budget $P_{i,j}$ ($\mathrm{m^2\,h^{-1}}$) for each pixel with the indices i, k in the x and z directions, respectively, at time step n is estimated using

$$P_{i,k}^{n} = \pm P_{\mathrm{e}}^{n} \pm P_{\mathrm{w}}^{n} \pm P_{\mathrm{u}}^{n} \pm P_{\mathrm{d}}^{n}. \tag{9}$$

HESSD
12, 5123–5149, 2015

Note, the sign of power across the cell faces depends on the direction of the fluxes i.e. inward fluxes result in an export of power (negative sign), while outward fluxes result in an import of power (positive sign) (Schymanski et al., 2010).

At dynamic equilibrium, the annual net power over the simulation time of one year at each grid point, $\overline{P}_{i,j}$ ($m^2\,a^{-1}$) is obtained via summation of $P_{i,j}$

$$\overline{P}_{i,k} = \sum_{n=1}^{NT} P_{i,k}^{n}. \tag{10}$$

Consistent with Eq. (5), the net power over different regions of the computational domain, $\overline{P}$ ($m^2\,a^{-1}$), such as the two recharge and discharge halfspaces, may be obtained via

$$\overline{P} = \sum_{i}^{NI} \sum_{k}^{NK} \overline{P}_{i,k}, \tag{11}$$

where NK is the upper bound in the z direction.

3 Results

3.1 General observations and optimality

In a first step, a straightforward mass balance calculation was performed for all simulated cases, which shows that PCP = E over the entire domain and one year simulation period at dynamic equilibrium. Interestingly, a groundwater reservoir is generated in the simulations under semi-arid atmospheric forcing, which connects a recharge zone with a discharge zone with $-\overline{q}^{ev} = \overline{q}^{inf}$, both developing naturally in the numerical experiment forming a large-scale circulation pattern (Fig. 1). In case of S2,

HESSD
12, 5123–5149, 2015

this large-scale circulation pattern is underlying a number of small-scale circulations patterns originating from the random heterogeneity in K_{sat}.

In Fig. 1, the cross section of $\overline{H}_{i,j}$ is plotted for S1 and S2 for $K_{sat} = 0.005$ ($m\,h^{-1}$). At the top (the land surface) the net fluxes of the recharge and discharge zones $\overline{q}^{inf}$ and $\overline{q}^{ev}$ are indicated separating the hillslope into two half-spaces. Note, that $\overline{H}_{i,j}$ decreases monotonously from $z = 0$ at the bottom toward the land surface *everywhere* in the domain. Thus, the average gradient of $\overline{H}_{i,j}$ does not point into the direction of the mean vertical flux in the recharge zone. This is not intuitive, but physically meaningful and can be explained with the nonlinear nature of the Darcy flow under variably saturated conditions due to the dependence of the relative hydraulic conductivity, $k_r(p)$, on the hydraulic pressure, p: under wet conditions, vertical moisture fluxes toward the water table are large with small gradients, while under dry conditions, fluxes are small with large gradients. Eventually the saturated zone is disconnected from ensuing drying events at the surface, because of the well-known processes of three-stage evaporation (Or et al., 2013). The nonlinear dynamics of these processes are effectively simulated, because of the high spatial discretization of $\Delta z = 1$ cm in the vertical direction, and constitute an important degree of freedom in the ensuing power analyses. This rather simple but non-trivial finding has major implications for the analysis of coupled nonlinear systems. Because the mean potential gradients may not point into the direction of the mean flux, it is arguably impossible to arrive at effective exchange coefficients in a straightforward manner. This is discussed in detail in Sect. 3.2 including a possible solution approach.

Figure 2 shows net power $\overline{P}$, of the dynamic equilibrium simulation for $K_{sat} = 0.005$ ($m\,h^{-1}$) for the homogenous S1, and heterogeneous, S2, experimental setup. In case of S1, the cross section exhibits characteristic regions of $\overline{P}$ export and import. The lower part of the domain below approximately 2.5 m corresponds to the groundwater reservoir with the recharge zone on the right and the discharge zone on the left. During precipitation events, this reservoir is connected episodically with the intermediate zone

HESSD
12, 5123–5149, 2015

above, which is a general net exporter of power (i.e. zone of net inflow) from net recharge in the right halfspace and capillary rise in the left halfspace. This zone is separated at the top by a distinct band of low power from an active zone of approximately 0.5 m thickness, which is in constant interaction with the atmospheric forcing i.e. evaporation and infiltration at the land surface. Note, in this active zone, the red vertical segments of $\overline{P}$ correspond to subtle but abrupt changes in the topography due to the finite difference/control volume approximation in PF.CLM. This is not a numerical arte fact, but a result of the stair-step like topographic representation at the centimeter scale. At these locations strong lateral gradients are generated, which are especially pronounced under dry conditions and explicitly resolved, because of the extremely high spatial resolution of the model.

In case of S2, the spatial white noise perturbation of K_{sat} results in additional small-scale recharge-discharge zones and circulation patterns at the surface and deeper subsurface superposed on the large-scale pattern, which is obtainable for S2 via mass balance calculation for the recharge and discharge halfspaces. The band of zero net power separating the active zone from the deeper subsurface is less well defined and located at greater depth on average. Additionally, the recharge and discharge zones of the intermediate and deeper subsurface i.e. the groundwater reservoir are perturbed and not identifiable anymore from the net power cross section.

Figure 3 shows an example of two vertical profiles for S1 and S2 of absolute values of power, $\log(|\overline{P}|)$, extracted from the recharge halfspaces of the cross sections provided in Fig. 2. While the vertical zonation is similar in both cases, the homogeneous conditions of S1 generally result in considerably smaller $\overline{P}$ values especially in the groundwater reservoir. In addition, heterogeneity in K_{sat} strongly smooths the profile, but the different zones (e.g., the active zone) are still recognizable.

Figure 4 summarizes the results of the analysis over the recharge/discharge zone with respect to net power, $\overline{P}$; the net Darcy flux $-\overline{q}^{\mathrm{ev}} = \overline{q}^{\mathrm{inf}} = \overline{q}$; and the spatiotemporal

HESSD
12, 5123–5149, 2015

mean of the hydraulic head at the bottom of the domain, $\overline{H}_{bot}$; all as a function of $\log(K_{sat})$. Note, in Fig. 4c, $\overline{q}$ is normalized by K_{sat}.

In Fig. 4a, net power, $\overline{P}$, is plotted, which shows clear maxima at around $\log(K_{sat}) = -2$ and $\log(K_{sat}) = 0$ for scenario S1 and S2. Net power is also generally larger under heterogeneous conditions of S2. Note that power increases sharply for $\log(K_{sat}) > -1$, when the groundwater reservoir falls dry in the simulations. This is reflected in Fig. 4d, when $\overline{H}_{bot} < 0$, which is indicated as the grey areas in Figs. 4 and 5.

It is remarkable that the critical zone indeed appears to exhibit maximization in the generation of power by adjusting the flux and force (gradient) accordingly. In this adjustment, the groundwater reservoir with its free water table is critical as a degree of freedom in the nonlinear problem of unsaturated flow. While the flux increases monotonically with increasing K_{sat} until the groundwater reservoir falls dry between $\log(K_{sat}) = -1$ and -0.3 (Fig. 4b and c), power does not increase monotonically resulting in the first maximum. Because the water table depth increases with increasing K_{sat}, the groundwater reservoir is further disconnected from the land surface (Fig. 4d) leading to dryer conditions in the hillslope. Thus, there are competing processes involved that result in a maximization of power: while there is increasing circulation in the hillslope with increasing K_{sat} (Fig. 4b and c), the water table drops and the hillslope becomes drier and *less efficient* in the generation of power. This implies that the effective force, $\Delta\overline{H}$, which drives the flux and power in competition with the flux, needs to decrease for $\log(K_{sat}) > -2$.

The second maximum in $\overline{P}$ at around $\log(K_{sat}) = 0$ occurs with a continuing decrease of $\overline{q}$ and manifests the transition to a completely different flow geometry without a groundwater reservoir and only variably saturated flow. Therefore, the mechanisms are determined by the internal dynamics of the system and also by the (no-flow) boundaries. The correct location of this "discontinuity" may be further resolved with additional simulations. Note, at this point of the discussion some caution is appropriate, because $\overline{P}$ exhibits maximization with respect to K_{sat} and not with respect to an

HESSD
12, 5123–5149, 2015

effective exchange or conductance coefficient, $\overline{\lambda}$, which is not available at this point, but will be derived below.

An additional important observations must be made: $\overline{H}_{bot}$ values are almost identical for small K_{sat} values in S1 and S2 and differ only slightly for larger K_{sat} values. Thus, while the mean fluxes are strongly dependent on heterogeneity, the mean water table location is mostly a function of the homogenous and geometric K_{sat} in S1 and S2, respectively. Because the free water table is a measurable quantity, important in the maximization of $\overline{P}$, and apparently relatively independent from heterogeneity, $\overline{H}_{bot}$ may be useful in the identification of an effective conductance $\overline{\lambda}$. This hypothesis is also further tested below.

It is also interesting that the power and fluxes are significantly larger in case of heterogeneity, while the location of the water table does not change considerably. This is due to additional circulation cells that are generated by the perturbation of K_{sat}, which generate longer flow paths resulting in a more effective dissipation of incoming energy i.e. water flux at the land surface. Thus, heterogeneity (or chaos) in hydraulic properties is effective in the dissipation of energy similar to turbulence in fluid dynamics. The question is whether this is due to larger effective conductances and/or larger effective forces in case of heterogeneity, which will be addressed below.

3.2 MEP principle as an inference tool

Ultimately, the appeal of MEP (or EPO principles in general) are the inference of upscaled or effective exchange coefficients and forces/gradients, which may be used to quantitatively describe the complex system without the explicit knowledge about microscopic details (Dewar, 2009). In this context, a popular example is gas diffusion, which can be captured by an inferred, macroscopic diffusion coefficient and gradient instead of honoring the motion and interactions of individual molecules. However, in hydrologic applications, it is not obvious how MEP may be useful in this sense.

HESSD
12, 5123–5149, 2015

Here, an attempt is made to conceptually transfer the numerical, "microscopic" hillslope model into a macroscopic conceptual model (Fig. 5) directed at Kleidon and Schymanski (2008) and Westhoff et al. (2014). In the conceptual model, the infiltration and evaporation flux, q_{inf} and q_{et}, are obtained from the hillslope model (e.g., Fig. 1). From the water and power budget analysis the macroscopic flux, $\overline{q} = \overline{q}^{ev} = \overline{q}^{inf} = q_{et} = q_{inf}$, and power $\overline{P}$ are available under dynamic equilibrium conditions. What is missing are the macroscopic heads of the conceptual model $H_{b,h}$ and $H_{b,l}$, or the corresponding macroscopic force $\Delta\overline{H} = H_{b,h} - H_{b,l}$.

In the numerical experiment, the instantaneous force $\Delta H = (H_h - H_l)$ is clearly defined at the local scale as the difference in hydraulic head between neighboring cells (Eq. 7). However, at the macroscopic scale of the bucket model, the upscaled, macroscopic force $\Delta\overline{H}$ is not easily derived from the numerical experiment. Due to the nonlinear nature of variably saturated flow, simple spatiotemporal averaging of hydraulic head over the recharge and discharge halfspaces of the hillslope model will not lead to meaningful gradients or forces. As a matter of fact, this type of averaging may lead to mean gradients pointing in the opposite direction of the flux as discussed in the context of Fig. 1. In addition, an upscaled effective exchange or conductance coefficient, $\overline{\lambda}$ is not available. Thus, one is left with two unknowns ($\Delta\overline{H}$ and $\overline{\lambda}$) and only one equation that is Darcy's law. This is generally the case in subsurface hydrology when dealing with the upscaling problem.

Yet, with $\overline{P}$ and $\overline{q}$ at hand, which were calculated directly from the "microscopic" simulations, a rather intuitive solution is to apply Eq. (2) and solve directly for $\Delta\overline{H} = \overline{P}/\overline{q}$ (L), which is shown in Fig. 6a as a function of $\log(K_{sat})$. Because $\overline{q}$ decreases faster than $\overline{P}$, $\Delta\overline{H}$ has a maximum at $\log(K_{sat}) = -3$. Thus, $\overline{P}$ may also be interpreted as an upscaled force weighted by the corresponding flux. This type of weighing is very useful, because in case of Richards equation, under dry conditions, small fluxes correspond with large gradients, while under wet conditions, large fluxes correspond

HESSD
12, 5123–5149, 2015

with small gradients. In order to arrive at an upscaled gradient, $\nabla\overline{H}$, $\Delta\overline{H}$ may be divided by a characteristic length scale, L, that is e.g. the length of the hillslope.

In the next step, applying Darcy's or conductance law to Eq. (2), one may additionally solve for a macroscopic or effective conductance coefficient $\overline{\lambda} = \overline{P}/\Delta\overline{H}^2$ (T^{-1}), which was unseizable before (Fig. 6b). Thus, MEP provides a second equation in addition to Darcy's law to solve for the two classic unknowns that are the effective gradient and exchange coefficient in the problem of upscaling of nonlinear hydrologic systems. Interestingly, $\overline{\lambda}$ does not change significantly between the homogenous, S1, and perturbed K_{sat}, S2 case considering a SD of one order of magnitude in the perturbation for S2. It appears that the system equilibrates at very similar effective exchange coefficients in case of small-scale chaos. Figure 4b also sheds light on the initial assumption that K_{sat} is proportional to $\overline{\lambda}$, which holds for $\log(K_{sat}) < -1$. In case of no groundwater reservoir and $K_{sat} > -1$, $\overline{\lambda}$ is inversely proportional to K_{sat}, because of the strong nonlinearity in the relative hydraulic conductivity in Richards equation.

In Fig. 4, $\overline{P}$ was plotted vs. K_{sat}, indicating but not yet demonstrating maximization of power. Figure 6c now demonstrates maximization by plotting the derived $\overline{\lambda}$ values vs. $\overline{P}$. Remarkably, the maxima of $\overline{P}$ occur at the same $\overline{\lambda}$ values in the presence and absence of a groundwater reservoir (solid and dashed lines respectively). Thus, the hillslope indeed maximizes power via attaining a unique optimized effective exchange coefficient for quite different hydrologic conditions. In case of heterogeneous conditions of S2, more power is obtained without a groundwater reservoir, which is reversed in comparison to S1, when slightly more power is obtained in the presence of a groundwater reservoir. The mean flux, $\overline{q}$, as function of $\overline{\lambda}$ shown in Fig. 6d behaves very similar in case of S1 and S2. Thus, a scaling law may be available with respect to the perturbation of K_{sat} collapsing both curves into one, which will require additional simulations of heterogeneous hillslopes.

HESSD
12, 5123–5149, 2015

Figure 6 also answers the questions posed in the previous section. Because $\Delta\overline{\lambda}$ increases monotonously until the groundwater reservoir disappears, the maximum in the effective force $\Delta\overline{H}$ is responsible for the first maximum in $\overline{P}$. The second maximum is also mainly determined by $\Delta\overline{H}$, when $\overline{\lambda}$ decreases, because of the changes in the overall flow geometry without a free water table. The increase in the flux due to the perturbation of K_{sat} can also be attributed mainly to an in increase in local and upscaled effective forces shown in Fig. 6a.

3.3 Open questions and suggested path forward

The results from the numerical simulations suggest that MEP is indeed happening in a hillslope mainly due to the interaction of a free moving water table with the atmospheric forcing, and the associated strongly nonlinear soil moisture redistribution. However, it is not obvious how the results can be applied to real world systems. For example, power can not be measured in the field, thus, the second equation, which is needed to solve for an effective conductance coefficient or force, is not applicable directly to measurements; additional physics based simulation are required. However, the results suggest that the water table or hydraulic head at the bottom of an aquifer, $\overline{H}_{bot}$, as a measurable quantity plays a key role in MEP of hydrologic systems. In Fig. 7, plotting $\overline{H}_{bot}$ vs. $\overline{\lambda}$ demonstrates that the mean position of the water table (solid lines with symbols in Fig. 7) is indeed a good reflection of the effective state of conductance of the hillslope independent of heterogeneity. Thus, empirical relationships of $\overline{H}_{bot}$ with $\overline{\lambda}$ may be developed for different hillslope configurations and climate conditions, which may provide a way to arrive at effective gradients in case of known net fluxes (or vice versa). However, this clear relationship disappears, when the groundwater reservoir dries up and $\overline{H}_{bot} < 0$ (dashed lines with symbols in Fig. 7).

In this context, the limited set of simulations presented here does not provide general scaling relationships that could be used to relate, for example, net fluxes to estimates

HESSD
12, 5123–5149, 2015

of saturated hydraulic conductivity in order to arrive at an effective gradient. A large number of additional experiments will be required. These must also take into account different types of atmospheric forcing and topography, which will also impact the relationships presented here, because of the strong nonlinearity of the system under consideration. Additionally, vegetation and spatially correlated heterogeneity in all hydraulic parameters needs to be taken into account. Thus, there are a larger number of exciting research possibilities, which will lead to a more in-depth understanding of the applicability of the presented concepts.

4 Summary and conclusions

Utilizing results from high-resolution, physics-based simulations of a 2-D semi-arid hillslope, entropy production optimization and inference principles were tested under dynamic equilibrium conditions. The results suggest that power or entropy production is indeed maximized, because the force, which drives the flux and entropy production, is reciprocally depleted by the same flux. In this process, the free water table plays a key role. While the flux and the depletion of the gradient are increased by an increase in the saturated hydraulic conductivity, water table depth increases as well, which results in overall drier conditions in the hillslope. Because of the nonlinearity of variably saturated flow, this leads to a decrease in the effective force and resulting power. Thus, there is competition between an increasing flux and declining water table for varying effective hydraulic conductances, which constitutes an important degree of freedom in the maximization of entropy production.

It appears that due to this nonlinearity of variably saturated flow, there is very little opportunity for upscaling under realistic dynamic equilibrium conditions, because one is always left with one equation (Darcy's law) and two unknowns that are the effective conductance coefficient and effective force/gradient. In this dilemma, MEP may provide a second equation for obtaining the effective values and transferring the "microscopic"

HESSD
12, 5123–5149, 2015

model into a macroscopic model of reduced complexity, as was demonstrated in this study.

Transferring and validating the results with measurements is difficult, because entropy or power can not be observed and measured directly. Thus, additional physics-based simulations accounting for the required degrees of freedom and nonlinearities will be needed in conjunction with data. However, the mean depth of the water table appears to be a strong measure of the effective state of the hydrologic system reflected by an effective conductance coefficient.

The presented results are comprehensive in the sense that the pertinent physical processes are simulated and analyzed in a fully-coupled, mass and energy conservative fashion and consistent theoretical framework. However, the results are not exhaustive. They are a starting point for a rich set of physics-based simulations, analyses, and discussion in the suggested context, which need to be connected to observations in future. These simulations and analyses need to include e.g., vegetation, spatially correlated heterogeneity in subsurface and land surface properties, and varying climate conditions.

Acknowledgements. I would like to thank Michal Herbst for the helpful discussions on hillslope hydrologic and suggestions that improved the manuscript.

The article processing charges for this open-access publication were covered by a Research Centre of the Helmholtz Association.

References

Abe, S. and Okuyama, S.: Similarity between quantum mechanics and thermodynamics: entropy, temperature, and Carnot cycle, Phys. Rev. E, 83, 021121, doi:10.1103/Physreve.83.021121, 2011.

del Jesus, M., Foti, R., Rinaldo, A., and Rodriguez-Iturbe, I.: Maximum entropy production, carbon assimilation, and the spatial organization of vegetation in river basins, P. Natl. Acad. Sci. USA, 109, 20837–20841, doi:10.1073/Pnas.1218636109, 2012.

HESSD

12, 5123–5149, 2015

Dewar, R.: Information theory explanation of the fluctuation theorem, maximum entropy production and self-organized criticality in non-equilibrium stationary states, J. Phys. A-Math. Gen, 36, 631–641, Pii S0305-4470(03)34726-2, doi:10.1088/0305-4470/36/3/303, 2003.

Dewar, R. C.: Maximum entropy production as an inference algorithm that translates physical assumptions into macroscopic predictions: don't shoot the messenger, Entropy, 11, 931–944, doi:10.3390/E11040931, 2009.

Dewar, R. C.: Maximum entropy production and plant optimization theories, Philos. T. R. Soc. B, 365, 1429–1435, doi:10.1098/Rstb.2009.0293, 2010.

Ehret, U., Gupta, H. V., Sivapalan, M., Weijs, S. V., Schymanski, S. J., Blöschl, G., Gelfan, A. N., Harman, C., Kleidon, A., Bogaard, T. A., Wang, D., Wagener, T., Scherer, U., Zehe, E., Bierkens, M. F. P., Di Baldassarre, G., Parajka, J., van Beek, L. P. H., van Griensven, A., Westhoff, M. C., and Winsemius, H. C.: Advancing catchment hydrology to deal with predictions under change, Hydrol. Earth Syst. Sci., 18, 649–671, doi:10.5194/hess-18-649-2014, 2014.

Kleidon, A.: A basic introduction to the thermodynamics of the Earth system far from equilibrium and maximum entropy production, Philos. T. R. Soc. B, 365, 1303–1315, doi:10.1098/rstb.2009.0310, 2010.

Kleidon, A. and Schymanski, S.: Thermodynamics and optimality of the water budget on land: a review, Geophys. Res. Lett., 35, L20404, doi:10.1029/2008gl035393, 2008.

Kleidon, A., Zehe, E., Ehret, U., and Scherer, U.: Thermodynamics, maximum power, and the dynamics of preferential river flow structures at the continental scale, Hydrol. Earth Syst. Sci., 17, 225–251, doi:10.5194/hess-17-225-2013, 2013.

Kollet, S. J. and Maxwell, R. M.: Integrated surface-groundwater flow modeling: a free-surface overland flow boundary condition in a parallel groundwater flow model, Adv. Water Resour., 29, 945–958, doi:10.1016/J.Advwatres.2005.08.006, 2006.

Kollet, S. J. and Maxwell, R. M.: Capturing the influence of groundwater dynamics on land surface processes using an integrated, distributed watershed model, Water. Resour. Res., 44, W02402, doi:10.1029/2007wr006004, 2008.

Koutsoyiannis, D.: Entropy: from Thermodynamics to Hydrology, Entropy, 16, 1287–1314, doi:10.3390/E16031287, 2014.

Miedziejko, E. M. and Kedziora, A.: Impact of plant canopy structure on the transport of ecosystem entropy, Ecol. Model., 289, 15–25, doi:10.1016/J.Ecolmodel.2014.06.013, 2014.

HESSD

12, 5123–5149, 2015

Or, D., Lehmann, P., Shahraeeni, E., and Shokri, N.: Advances in soil evaporation physics – a review, Vadose Zone J., 12, doi:10.2136/vzj2012.0163, 2013.
Paillard, D. and Herbert, C.: Maximum entropy production and time varying problems: the seasonal cycle in a conceptual climate model, Entropy, 15, 2846–2860, doi:10.3390/E15072846, 2013.
Porada, P., Kleidon, A., and Schymanski, S. J.: Entropy production of soil hydrological processes and its maximisation, Earth Syst. Dynam., 2, 179–190, doi:10.5194/esd-2-179-2011, 2011.
Schymanski, S. J., Kleidon, A., Stieglitz, M., and Narula, J.: Maximum entropy production allows a simple representation of heterogeneity in semiarid ecosystems, Philos. T. R. Soc. B, 365, 1449–1455, doi:10.1098/Rstb.2009.0309, 2010.
Westhoff, M. C. and Zehe, E.: Maximum entropy production: can it be used to constrain conceptual hydrological models?, Hydrol. Earth Syst. Sci., 17, 3141–3157, doi:10.5194/hess-17-3141-2013, 2013.
Westhoff, M. C., Zehe, E., and Schymanski, S. J.: Importance of temporal variability for hydrological predictions based on themaximum entropy production principle, Geophys. Res. Lett., 41, 67–73, doi:10.1002/2013gl058533, 2014.
Zehe, E., Ehret, U., Blume, T., Kleidon, A., Scherer, U., and Westhoff, M.: A thermodynamic approach to link self-organization, preferential flow and rainfall–runoff behaviour, Hydrol. Earth Syst. Sci., 17, 4297–4322, doi:10.5194/hess-17-4297-2013, 2013.

HESSD
12, 5123–5149, 2015

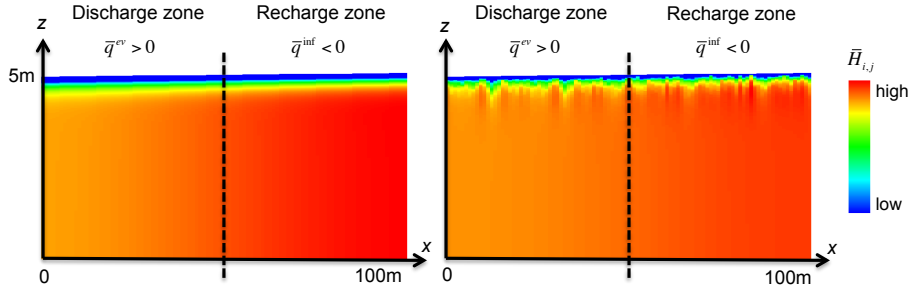

Figure 1. Mean hydraulic head cross-sections, $\overline{H}_{i,j}$, of S1 (left) and S2 (right) obtained from the dynamic equilibrium simulations. Indicated are the net recharge ($\overline{q}^{inf} < 0$) and discharge ($\overline{q}^{ev} > 0$) halfspaces. The color scale is indicated qualitatively, because of the wide range of hydraulic head values resulting from the semi-arid time series.

HESSD
12, 5123–5149, 2015

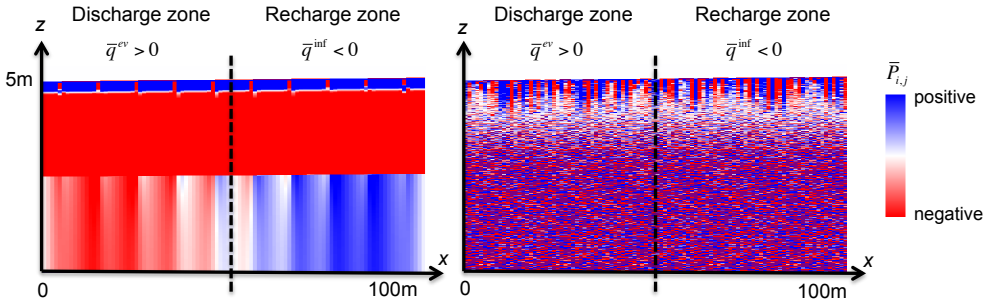

Figure 2. Example of net power, $\overline{P}_{i,j}$, of the dynamic equilibrium condition for K_{sat} = 0.005 and homogenous and heterogeneous conditions of the experimental setups S1 (left) and S2 (right), respectively.

HESSD
12, 5123–5149, 2015

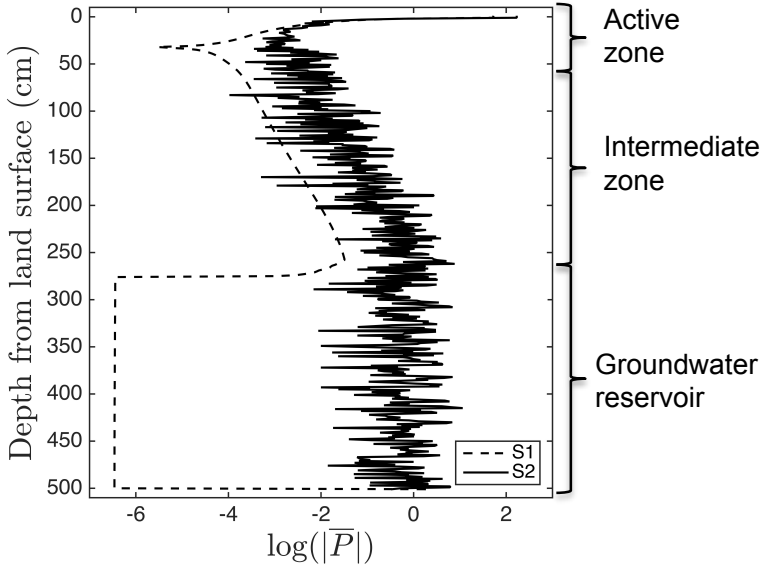

Figure 3. Vertical profile of log absolute power, log(|$\overline{P}$|), extracted from the discharge zone for the homogenous and heterogeneous scenario S1 and S2, respectively.

HESSD
12, 5123–5149, 2015

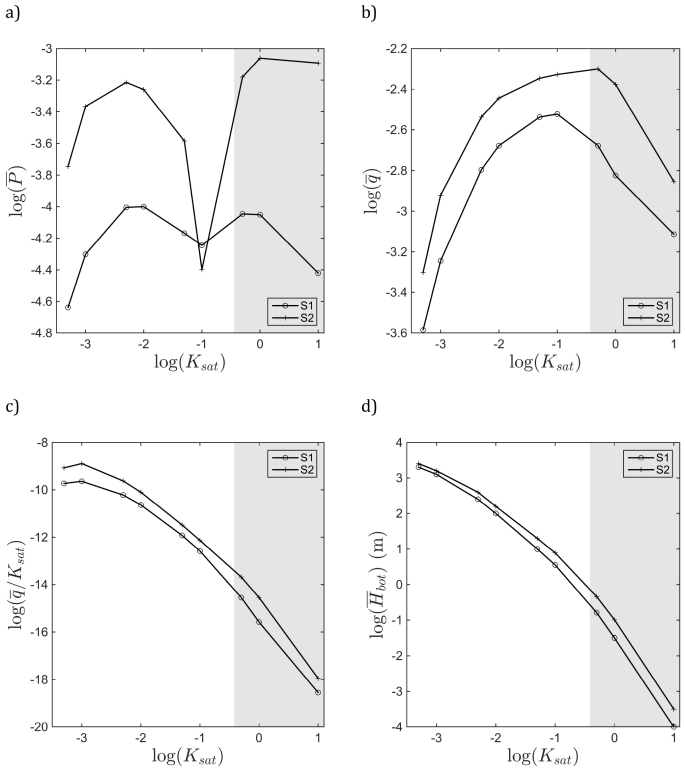

Figure 4. (a) Logarithm of net power, $\overline{P}$ ($m^2 a^{-1}$); **(b)** logarithm of net flux, $\overline{q}$ ($m a^{-1}$); **(c)** logarithm of $\overline{q}/K_{sat}$ (–); and **(d)** mean hydraulic head, $\overline{H}_{bot}$ (m), at the bottom of the cross section, all as a function of $\log(K_{sat})$ for the recharge/discharge halfspaces of the S1 and S2 experiments. The grey area indicates K_{sat} values at which the groundwater reservoir falls dry ($\overline{H}_{bot} < 0$).

HESSD
12, 5123–5149, 2015

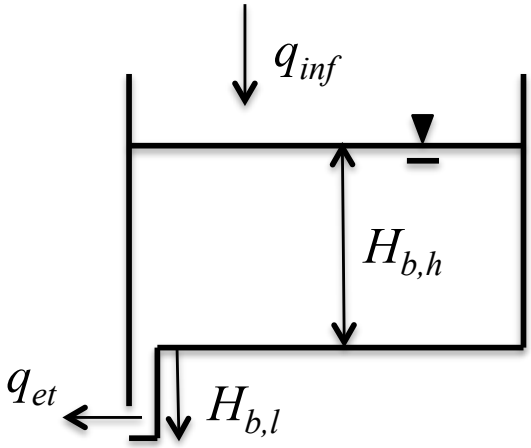

Figure 5. Macroscopic hillslope bucket model after Westhoff et al. (2014), where $H_{b,h}$ and $H_{b,l}$ are the unknown macroscopic hydraulic heads or potentials, and q_{inf} and q_{et} are the mean infiltration and evaporation fluxes obtained from the numerical experiments.

HESSD
12, 5123–5149, 2015

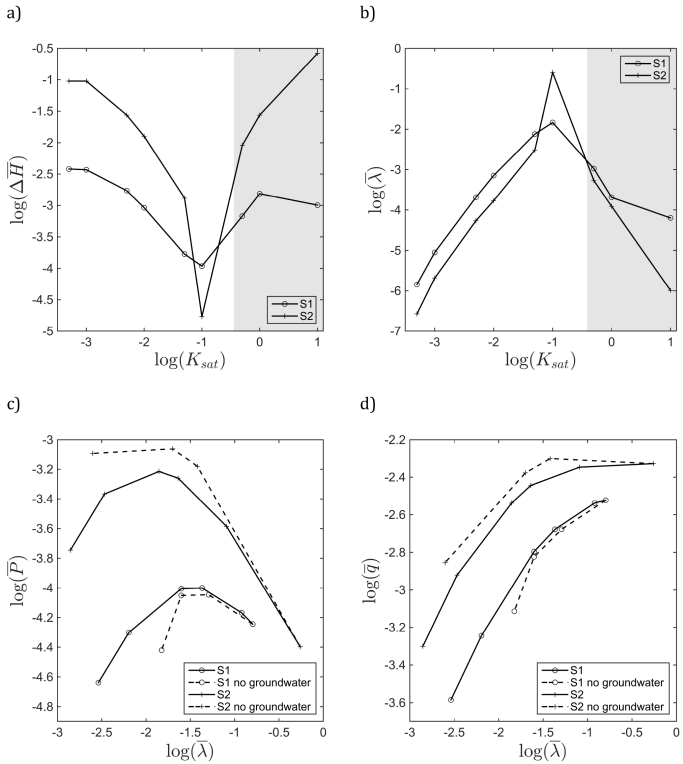

Figure 6. **(a)** Logarithm of the effective force, $\Delta\overline{H}$ (m); **(b)** logarithm of the effective conductance, $\overline{\lambda}$ (a^{-1}), as a function of $\log(K_{sat})$; and **(c)** power, $\overline{P}$ ($m^2\,a^{-1}$); and **(d)** mean flux, $\overline{q}$ ($m\,a^{-1}$), as a function of $\overline{\lambda}$ (a^{-1}). The grey areas in **(a)** and **(b)** indicate K_{sat} values at which the groundwater reservoir falls dry ($\overline{H}_{bot} < 0$). Similarly, in **(c)** and **(d)**, the solid and dashed lines indicate the presence and absence of a groundwater reservoir.

HESSD
12, 5123–5149, 2015

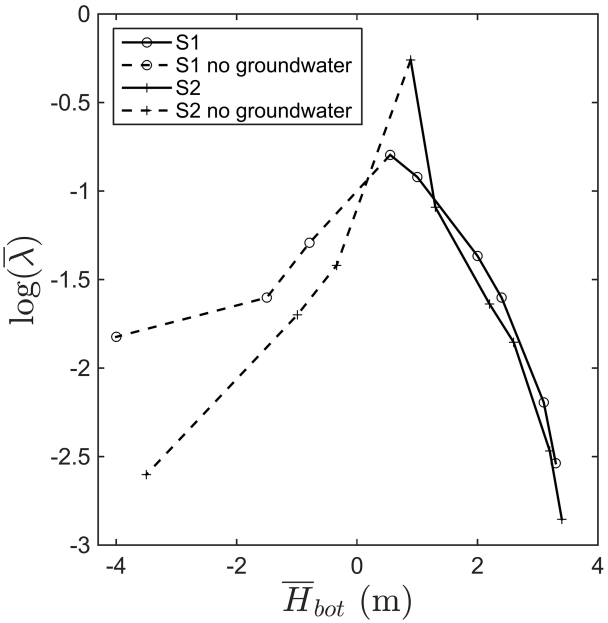

Figure 7. Effective conductance, $\overline{\lambda}$, plotted versus mean hydraulic head at the bottom of the simulation domain, $\overline{H}_{\text{bot}}$. Solid lines indicate the presence of a groundwater reservoir ($\overline{H}_{\text{bot}} > 0$), while dashed lines indicate the absence of a groundwater reservoir ($\overline{H}_{\text{bot}} < 0$).

HESSD
12, 5123–5149, 2015